Chinese Physics Letters

LETTER

Terahertz Pump-Terahertz Probe Spectroscopy Revealing Pockels and Kerr Effects in ZnTe

Cite as: Zhiqiang Lan *et al*. 2026 *Chin. Phys. Lett.* **43** 090402

DOI CSTR

Recommended Articles

Carrier Dynamics and Enhanced Terahertz Generation in GaAs Photoconductive Emitters with Microstructures
Yanrong Xiang, Zuanming Jin, Lei Hou, Zhiqiang Lan, Yang Li, Yan Peng, and Yiming Zhu
Chin. Phys. Lett. **42**, 110403 (2025)

100-mW High-Average-Power Strong-Field Terahertz Source
Ao-Jie Xu *et al*.
Chin. Phys. Lett. **42**, 120406 (2025)

Field-Induced Spin Continuum in Twin-Free $Na_3Co_2SbO_6$ Revealed by Magneto-THz Spectroscopy
Rongsheng Li *et al*.
Chin. Phys. Lett. **42**, 120711 (2025)

Electrically Tunable Graphene Terahertz Isolator Assisted by Nonreciprocal Plasmon
Chen-Ran Xu, Weiru Fan, Yanhao Tang, and Dawei Wang
Chin. Phys. Lett. **42**, 014201 (2025)

Symmetry-Driven Giant Magneto–Optical Kerr Effects in Altermagnetic Insulator
Jiaxin Luo, Xiaodong Zhou, Jinxuan Liang, Ledong Wang, Qiuyun Zhou, Yong Jiang, Wenhong Wang, Yugui Yao, Luyi Yang, and Wanjun Jiang
Chin. Phys. Lett. **43**, 020713 (2026)

A series journal of Chinese Physical Society distributed by IOP Publishing

Chinese Physics Letters

Chin. Phys. Lett. **43** 090402 (2026)

LETTER

DOI: 10.1088/0256-307X/43/9/090402
CSTR: 32039.14.0256-307X.43.9.090402

Terahertz Pump-Terahertz Probe Spectroscopy Revealing Pockels and Kerr Effects in ZnTe

Zhiqiang Lan(蓝志强)[1], Zuanming Jin(金钻明)[1,4,*], Jingyi Peng(彭静宜)[2], Tianxiao Nie(聂天晓)[2,*], Alexei V. Balakin[3], Alexander P. Shkurinov[3], Yan Peng(彭滟)[1,4,*], Yiming Zhu(朱亦鸣)[1,4,*], and Songlin Zhuang(庄松林)[1]

[1]National Key Laboratory of Terahertz Perception and Communication (TPCL), THz Technology Innovation Research Institute, THz Spectrum and Imaging Technology Cooperative Innovation Center, Shanghai Key Lab of Modern Optical System, University of Shanghai for Science and Technology, Shanghai 200093, China
[2]Fert Beijing Institute, MIIT Key Laboratory of Spintronics, School of Integrated Circuit Science and Engineering, Beihang University, Beijing 100191, China
[3]Faculty of Physics, Lomonosov Moscow State University, LeninskieGory 1, Moscow 119991, Russia
[4]Shanghai Institute of Intelligent Science and Technology, Tongji University, Shanghai 200092, China

*Corresponding authors. Email: physics_jzm@usst.edu.cn; nietianxiao@buaa.edu.cn; py@usst.edu.cn; ymzhu@usst.edu.cn

Terahertz (THz) pump–THz probe spectroscopy has emerged as a powerful platform for investigating ultrafast nonlinear light–matter interactions. However, the physical origin of recently reported THz signal enhancement remains controversial because contributions from THz generation and electro–optic detection are often coupled. Here, we use a Fe_4GeTe_2 spintronic THz emitter together with a ZnTe electro–optic detector to demonstrate that, with fixed THz pump polarity, reversing the magnetic-field direction of the Fe_4GeTe_2 emitter does not change the signal enhancement or induce suppression, indicating that the modulation originates from the nonlinear electro–optic response of the ZnTe detector rather than the THz emitter. Furthermore, controlling the polarity of the THz pump field reveals a pronounced asymmetric response: a positive THz field induces signal enhancement, whereas a negative field leads to suppression, revealing strong polarity-dependent THz pump–THz probe modulation. This behavior cannot be solely attributed to carrier redistribution in the conduction band and is consistently described by a model incorporating both linear Pockels and nonlinear Kerr effects in ZnTe. This polarity-dependent reversal of the linear Pockels contribution accounts for the observed polarity-dependent THz-field-induced absorption modulation. These results clarify the physical origin of THz pump–THz probe modulation, establish detection-induced nonlinearity as the dominant mechanism governing the measured response, and highlight the importance of treating electro–optic detection as an active nonlinear element in THz pump–THz probe spectroscopy.

Introduction

Since its emergence over half a century ago, nonlinear optics has evolved into a central branch of photonics [1]. While early studies primarily focused on the visible and infrared spectral regions, the development of intense terahertz (THz) sources has opened opportunities for exploring nonlinear optical phenomena at THz frequencies [2–4]. Located between the microwave and infrared regimes, THz waves combine low photon energies, deep penetration capability, and sub-picosecond temporal resolution [5–8]. In semiconductors, intense THz fields can drive free carriers into nonequilibrium states [9], enabling various nonlinear phenomena, including THz-modulated excitonic dynamics [10,11], impact-ionization-induced carrier multiplication [12,13], band-structure-dependent carrier transport [14–16], and ultrafast optical switching [17].

THz pump–THz probe (TPTP) spectroscopy has become a powerful approach for investigating THz nonlinear interactions. Early studies revealed intervalley scattering and carrier multiplication in semiconductors [18], hot-electron anisotropy effective mass arising from conduction-band nonparabolicity [19], THz-induced insulator-to-metal transitions in vanadium dioxide [20], and self-phase modulation associated with THz-driven carrier heating [21]. Sub-picosecond modulation was reported in doped semiconductors, where enhanced THz reflections at phonon overtones provided evidence of electron–phonon coupling [22]. TPTP spectroscopy was subsequently applied to monolayer graphene, where strong THz fields suppressed Faraday rotation through inter-Landau-level transitions [23]; silicon nanogaps exhibiting impact ionization and intervalley scattering [24]; AlGaN/GaN grating-gate structures showing plasmon-enhanced THz nonlinear absorption [25]; and superconducting Nb microstrips displaying current-driven superconducting–normal transitions [26]. Together, these studies highlight the ability of strong THz fields to manipulate matter on ultrafast timescales.

More recently, TPTP experiments have attracted increasing interest as a means of controlling THz fields on ultrafast timescales [27,28]. In 2022, spintronic THz pulses emitted from W/CoFeB/Pt heterostructures were used to modulate plasma-generated THz radiation through field-driven electron dynamics [29]. In 2024, plasma-based THz modulators achieved picosecond-scale amplification and extinction of broadband THz signals through dipole phase control [30]. Recent studies showed that co-propagating THz pulses can induce nonlinear polarization in ZnTe, leading to modifications of its electro–optic response. Based on this mechanism, a second-order nonlinear model was established and the effective third-order susceptibility $\chi^{(3)}(\omega_{\mathrm{THz}})$ was extracted [31]. Because THz pump and probe pulses simultaneously participate in both THz generation and electro–optic detection processes, distinguishing these contributions experimentally remains challenging. In particular, it remains unclear whether the observed modulation originates from the THz generation process or from linear/nonlinear effects occurring during THz detection. Furthermore, the roles of the amplitude and polarity of the modulating THz field in shaping the detected THz response are not yet fully understood. Resolving these issues is essential for clarifying the origin of TPTP experiments and for advancing ultrafast THz control technologies.

In this work, we employ a Fe_4GeTe_2 THz emitter and a ZnTe electro–optic detector to investigate the origin of TPTP modulation. By independently separating the THz generation and detection pathways,

Received 7 July 2026; accepted 14 August 2026; published 7 September 2026
© 2026 Chinese Physical Society and IOP Publishing Ltd. All rights, including for text and data mining, AI training, and similar technologies, are reserved.

Check for updates

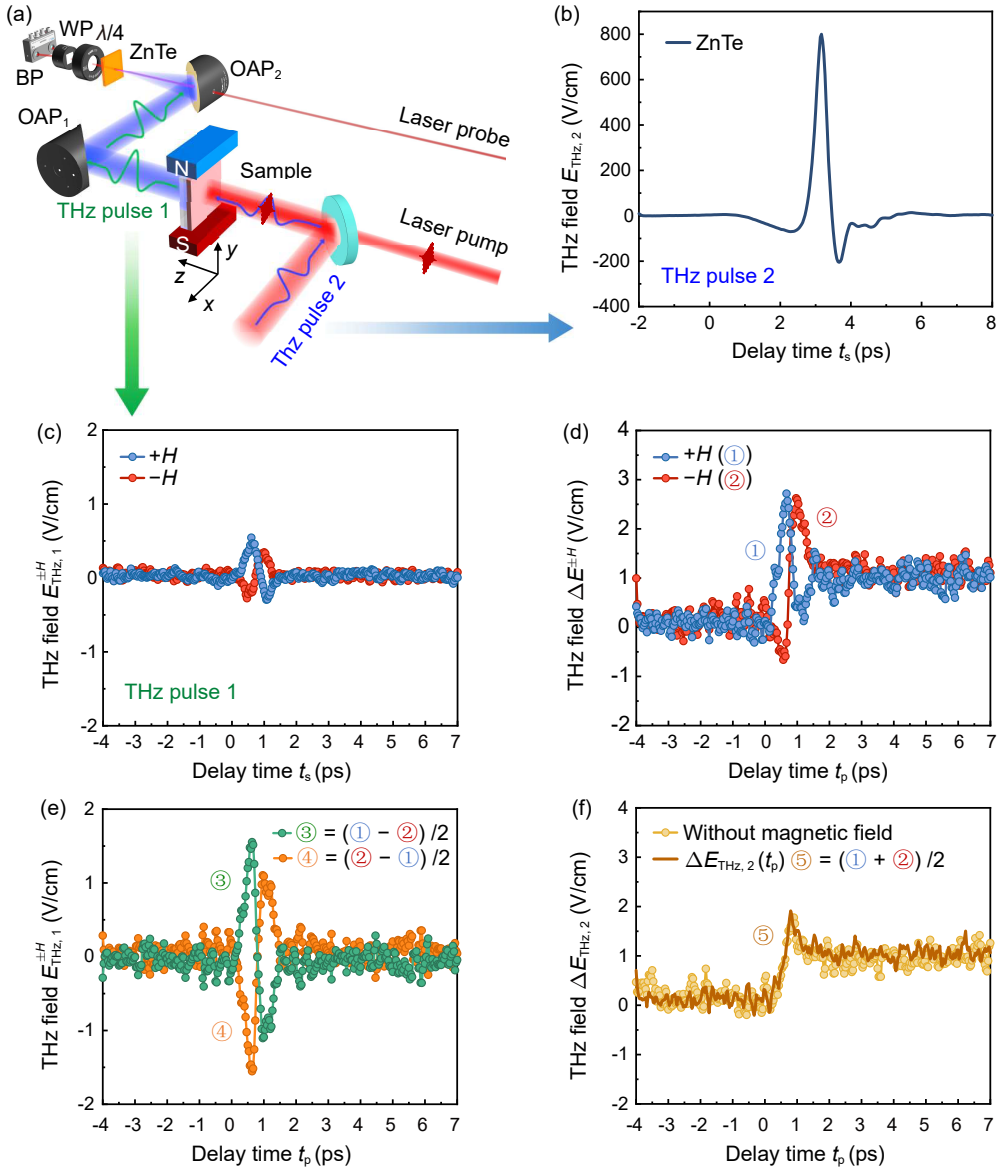

Fig. 1. (a) Schematic of the TPTP experiment setup (OAP: off-axis parabolic mirror; $\lambda/4$: quarter-wave plate; WP: Wollaston prism; BP: balanced photodiodes). (b) THz pulse 2 generated from ZnTe under 800 nm laser excitation at a pump fluence of 0.56 mJ/cm^2, with a peak field strength of ~800 V/cm. (c) THz pulse 1 emitted from Fe_4GeTe_2 film under $\pm H$ at a pumping fluence of 1.13 mJ/cm^2. (d) Photoinduced THz field modulation signal $\Delta E^{\pm H}$ of Fe_4GeTe_2 under $+H$ (blue line) and $-H$ (red line). (e) The reconstructed THz pulse 1 emission from Fe_4GeTe_2 film under $\pm H$. (f) The reconstructed peak transmission change of THz pulse 2, compared with the OPTP measurement without a magnetic field (yellow line).

we unambiguously demonstrate that the observed TPTP modulation originates from the ZnTe detection crystal rather than from the THz generation process. By systematically tuning the strength, polarity, and temporal delay of the THz pump pulse, we establish the key role of THz-induced linear and nonlinear effects in ZnTe.

Preparation of Samples

A 10 nm-thick Fe_4GeTe_2 film was grown on a 500 μm-thick Al_2O_3 substrate by molecular beam epitaxy under an ultrahigh-vacuum base pressure of $\sim 1\times10^{-10}$ Torr. Prior to deposition, the substrate was annealed at 600 ℃ to obtain a clean and well-ordered surface. The film was then synthesized via co-evaporation of high-purity Fe, Ge, and Te from standard Knudsen effusion cells, with carefully controlled fluence ratios. To protect the film from environmental degradation and damage during subsequent processing, a ~2 nm Ge capping layer was deposited on top. The XRD characterization of the sample was shown in previous work [32].

Experimental Setup

Figure 1(a) illustrates the configuration for TPTP measurements. The laser source is an amplified Ti:sapphire system delivering 120 fs pulses centered at 800 nm with a 1 kHz repetition rate and up to 7 W output power. Using this setup, we investigated THz-field-induced modulation of THz pulses generated from Fe_4GeTe_2 thin films. A 200 mT in-plane static magnetic field was applied along the y-axis to fully saturate the magnetization of the Fe_4GeTe_2 film. A femtosecond pump laser with a photon energy of 1.55 eV excites the Fe_4GeTe_2 film, generating a broadband THz pulse beam 1 (green). Meanwhile, another THz pulse beam 2 (blue), generated by a ZnTe crystal, is delivered collinearly with the pump laser onto the film. The intensity and polarity of the incident THz pulse beam 2 can be independently controlled. The transmitted blue THz pulse 2 and the green THz pulse 1 emitted from the Fe_4GeTe_2 film propagate collinearly and finally reach a 1-mm-thick ⟨110⟩-ZnTe electro–optic sampling (EOS) crystal. The chopper is placed in the THz pulse 1 path, so that the measured signal includes both the THz pulse 1 and the change of the THz

pulse 2. A delay stage was employed to control the time delay t_p of the optical pump pulse relative to THz pulse 2 as they propagate through the Fe_4GeTe_2 film. A second delay stage was used to control the time delay t_s of THz pulse 2 relative to the optical sampling pulse. If no THz is generated by the sample, the setup becomes a conventional optical pump–THz probe (OPTP) system [33−35]. All measurements were performed at room temperature under a dry-air purge to minimize THz absorption caused by atmospheric water vapor.

Experimental Data Analysis

Without the Fe_4GeTe_2 sample in the optical path, we first characterized the THz pulse 2, $E_{THz,2}(t_s)$, generated by the ZnTe crystal. Figure 1(b) shows the THz pulse 2 generated by a ZnTe crystal, with a peak electric field strength of ~800 V/cm (measured by moving the chopper). The calculation method of THz field strength is shown in the Supplementary Materials (SM) [36,37], which is in the same order of magnitude as the peak THz electric field strength of 687 V/cm previously reported for ZnTe [38]. Secondly, we blocked the THz pulse 2 and excited the Fe_4GeTe_2 sample with the laser pump pulse. Figure 1(c) shows the THz pulse 1 generated from the Fe_4GeTe_2 film grown on an Al_2O_3 substrate. Reversing the applied magnetic field by 180° flips the polarity of the emitted THz pulse 1. For a detailed discussion of the THz radiation mechanism, please refer to our previous study [32]. We then fixed the EOS sampling delay at the peak of the THz pulse 2 and scanned the delay time t_p between the laser pump pulse and the THz pulse 2. Figure 1(d) records the photoinduced THz field modulation signal $\Delta E^{\pm H}(t_p)$ under $+H$ (marked as ①) and $-H$ (marked as ②), which consists of two components: the transmitted change of THz pulse 2 and the emitted THz pulse 1 from the Fe_4GeTe_2 film [39],

$$\Delta E^{\pm H}(t_p) = E^{\pm H}_{THz,1}(t_p) + \Delta E_{THz,2}(t_p), \tag{1}$$

where $E^{\pm H}_{THz,1}(t_p)$ describes the THz emission from the optically excited Fe_4GeTe_2 film, with $\pm H$ representing the opposite applied magnetic fields. Meanwhile, $\Delta E_{THz,2}(t_p)$ represents the transient change in the peak value of THz pulse 2 induced by optical pumping. $\Delta E_{THz,2}(t_p) = E^{on}_{THz,2} - E^{off}_{THz,2}$ is obtained from the difference between the transmitted THz pulse 2 with and without pump laser excitation, i.e., $E^{on}_{THz,2}$ and $E^{off}_{THz,2}$, respectively. The $\Delta E_{THz,2}(t_p)$ is magnetic-field independent. Thus, we can disentangle $E^{\pm H}_{THz,1}(t_p)$ and $\Delta E_{THz,2}\left(t_p\right)$,

$$E^{\pm H}_{THz,1}(t_p) = \frac{1}{2}\left[\Delta E^{\pm H}(t_p) - \Delta E^{\mp H}(t_p)\right], \tag{2}$$

$$\Delta E_{THz,2}(t_p) = \frac{1}{2}\left[\Delta E^{+H}(t_p) + \Delta E^{-H}(t_p)\right]. \tag{3}$$

Based on Eqs. (2) and (3), we extract $E^{\pm H}_{THz,1}(t_p)$ of the Fe_4GeTe_2 film under $\pm H$ fields, as marked ③ and ④ in Fig. 1(e). In addition, $\Delta E_{THz,2}(t_p)$, derived from Eq. (3) (marked as ⑤), is in good agreement with the OPTP signal measured under zero magnetic field, as shown in Fig. 1(f). A comparison between Figs. 1(c) and 1(e) shows that, under the same optical pump fluence, the THz emission signal from the Fe_4GeTe_2 film pumped with THz pulse 2 is significantly larger than that measured without THz pulse 2 pumping.

To clarify whether the observed enhancement in THz amplitude arises from either the Fe_4GeTe_2 film or the ZnTe sampling crystal, we reversed the magnetization direction of the Fe_4GeTe_2 film. If this effect originates from the Fe_4GeTe_2 film, the positive and negative magnetic fields would generate charge currents with opposite polarities. For the fixed electromagnetic field of THz pulse 2, if it enhances the THz pulse 1 generation under a positive magnetic field, it must suppress the THz pulse 1 under a negative magnetic field. In other words, under modulation by THz pulse 2, THz pulse 1 is expected to exhibit opposite modulation trends under positive and negative magnetic fields. However, as shown in Figs. 1(c) and 1(e), the experimental observations reveal a distinct behavior: the amplitude of THz pulse 1 is consistently enhanced irrespective of the polarity of the applied magnetic field. This observation reveals that the ultrafast modulation of THz pulse 1 originates not from spin-mediated THz generation within the Fe_4GeTe_2 film, but from linear and nonlinear modulation effects in the ZnTe sampling crystal, as elaborated below.

We would like to note that Fe_4GeTe_2 was selected as the THz emitter because it provides a suitable THz field strength and enables magnetic-field-controlled reversal of the THz emission polarity. Under our experimental conditions, the peak THz electric field generated by Fe_4GeTe_2 is more than two orders of magnitude lower than that generated by ZnTe. This large difference in THz field strength is essential for our TPTP measurements. On the one hand, the relatively weak THz emission from Fe_4GeTe_2 minimizes additional nonlinear electro–optic responses in ZnTe. On the other hand, in OPTP measurements, it allows the photoinduced modulation of the THz probe signal to be distinguished from the THz radiation directly emitted by the photoexcited Fe_4GeTe_2, as shown in Fig. 1(d). The magnetic-field-controlled polarity reversal of Fe_4GeTe_2 provides an effective approach to identify the origin of the observed THz modulation and separate the emitter-related signal from the detector-induced nonlinear electro–optic responses.

In what follows, we concentrate on the THz pulse 2 pump and THz pulse 1 probe configuration implemented in the ZnTe sampling crystal, with the experimental geometry presented in Fig. 2(a). Our setup enables easy spatial and temporal overlap of the two THz pulses. To explore the origins of this ultrafast modulation of the THz emission, we excluded the magnetic field contribution and derived the THz signal by taking the difference between time-domain waveforms acquired under positive and negative magnetic fields [Eq. (2)]. The THz electric fields obtained with and without THz pulse 2 pumping the ZnTe crystal are denoted as $E_{THz}(t_p)$ and $E_{THz,1}(t_p)$, respectively. In the measurement, THz pulse 2 was always fixed at its peak position, while THz pulse 1 was recorded by scanning the time delay t_p. Figure 2(b) shows an experimental configuration in which the amplitude of THz pulse 1 is changed while the amplitude of THz pulse 2 is kept fixed. Figure 2(c) shows the pseudo-color map of the THz time-domain waveform for different t_p relative to the fixed THz pulse 2, as a function of pump laser fluence. As shown in Fig. 2(d), in the absence of THz pulse 2 as the pump, we found that the peak field of THz pulse 1 rises from 0.37 V/cm to 1.61 V/cm as the pump laser fluence increases from 0.56 mJ/cm^2 to 2.83 mJ/cm^2. For the configuration with THz pulse 2 pumping the ZnTe crystal, the peak field of THz pulse 1 is higher than that obtained without THz pulse 2 pumping. The peak field of THz pulse 1 rises from 1.55 V/cm to 3.97 V/cm across the same pump laser fluence range. Experimental results demonstrate that THz pulse 2 pumping of ZnTe substantially enhances the detection of THz pulse 1 radiated by Fe_4GeTe_2 films.

To further clarify the mechanism responsible for the observed THz pulse 1 signal enhancement, we kept the incident pump fluence of THz pulse 1 constant while tuning both the peak electric field strength and the polarity of the THz pumping pulse 2, as illustrated in Fig. 3(a). The electric field strength is controlled using a pair of wire-grid polarizers, while the field polarity is tuned by rotating the azimuthal angle of the ZnTe crystal. The time-domain THz waveforms plotted in Fig. 3(b) display amplified signals under positive THz pumping, whereas suppressed responses emerge upon negative-polarity THz excitation. Figure 3(c) reveals that the peak field of THz pulse 1 strongly depends on both the electric-field strength and polarity of the pumped THz pulse 2. Without excitation of THz pulse 2 on the ZnTe crystal, the peak field of THz pulse 1 is ~0.53 V/cm (green dashed line). When the THz pulse 2 is set to positive-polarity, the rising electric field strength drives the peak field of THz pulse 1 to increase from 0.53 V/cm to 2.88 V/cm. In contrast, negative-polarity THz pulse 2 reduces the peak field from 0.53 V/cm to 0.17 V/cm. These distinct trends confirm that the electric field of THz pulse 2 can either amplify or suppress the THz emission from the Fe_4GeTe_2 film.

Furthermore, figure 3(d) provides another modulation method: changing the relative time delay t_s between THz pulse 2 and the optical probe pulse. The incident pump fluence of THz pulse 1 remained

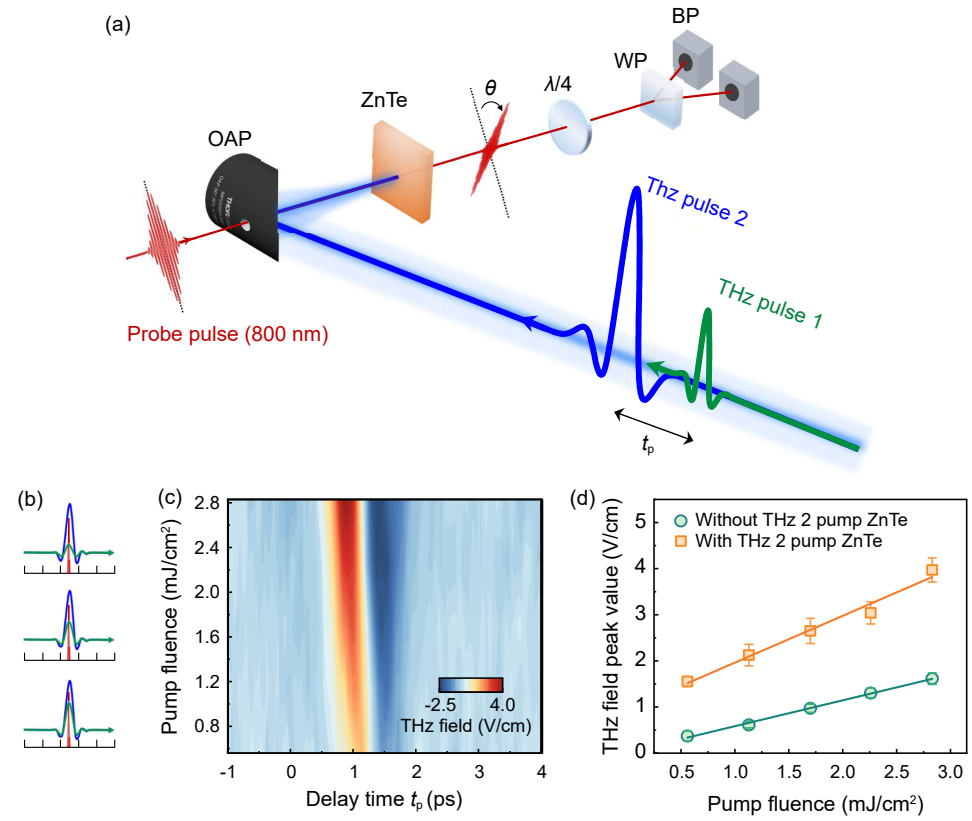

Fig. 2. (a) Schematic of the TPTP setup. THz pulse 1 (green) and THz pulse 2 (blue) propagate collinearly with controllable delay t_p, and the transmitted THz field is detected via EOS with an 800 nm probe pulse in ZnTe. (b) Schematic of a constant THz pulse 2 (blue) and varying the amplitude of THz pulse 1 (green). The optical probe pulse (red) is fixed at the peak of THz pulse 2. (c) Pseudo-color map of the THz time-domain waveform $E_{\mathrm{THz},1}(t_p)$ versus pump fluence (0.56 to 2.83 mJ/cm^2) with THz pulse 2 excitation on ZnTe. (d) The peak value of the THz field from the Fe_4GeTe_2 films as a function of pump laser fluence with and without THz pulse 2 excitation on ZnTe.

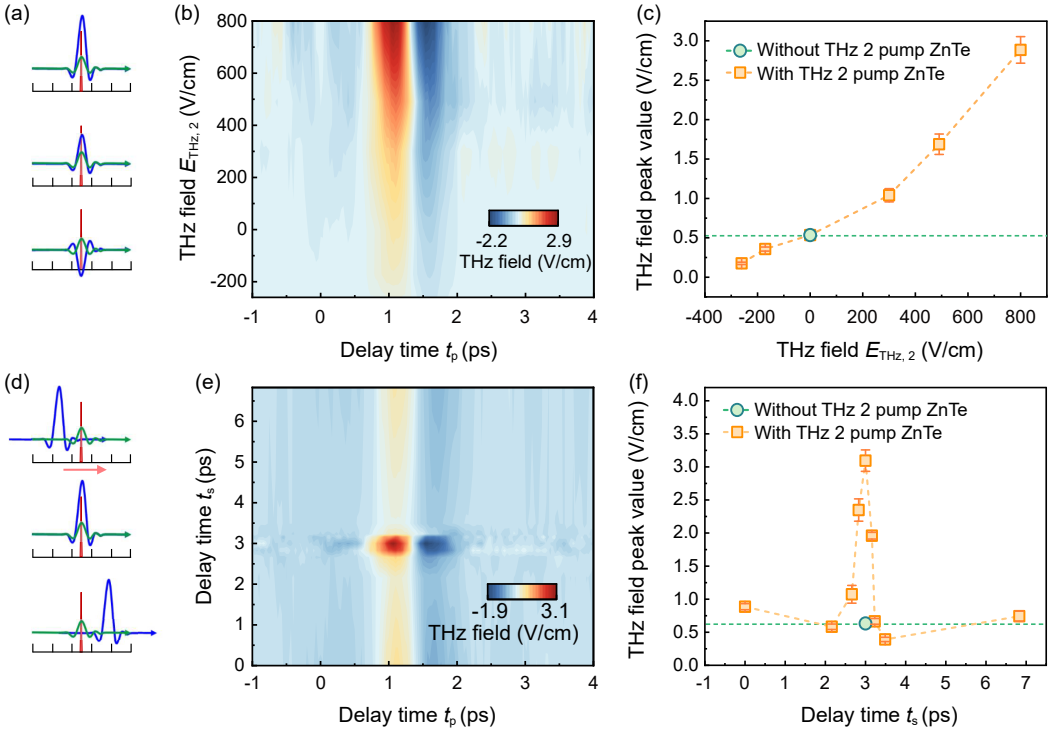

Fig. 3. (a) Schematic showing the tunable THz pulse 2 (blue) with variable field amplitude and polarity, THz pulse 1 (green), and optical sampling pulse (red). (b) Color plots of reconstructed THz time-domain waveforms measured under distinct peak field strengths of THz pulse 2. (c) Peak THz field amplitude versus the peak field of THz pulse 2, measured with and without THz pulse 2 pumping the ZnTe crystal. The pump field ranges from −260 to 800 V/cm. (d) Schematic illustrating the relative time delay t_s between THz pulse 2 (blue) and the optical sampling pulse (red). The THz waveform was scanned by t_p. (e) Color plots of reconstructed THz waveforms acquired at different time delays t_s. (f) Peak THz field amplitude as a function of $t_s = 0$, 2.16, 2.66, 2.83, 3, 3.16, 3.23, 3.49, 6.83 ps, recorded with and without THz pulse 2 excitation on the ZnTe crystal.

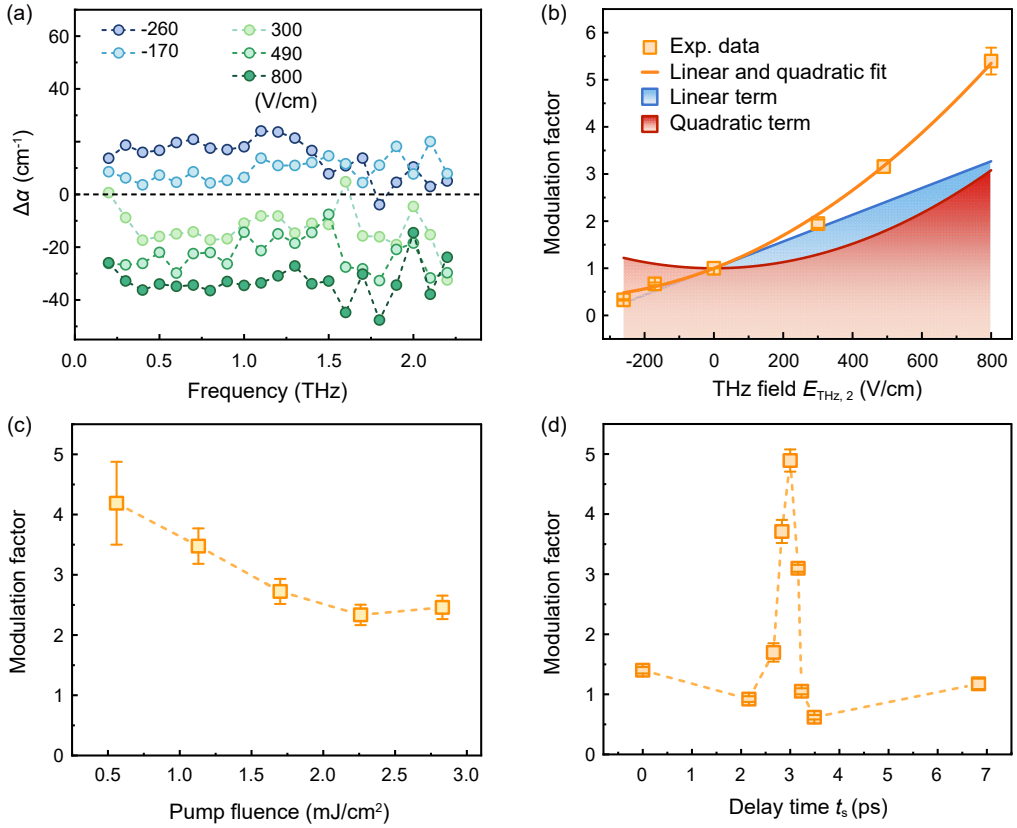

Fig. 4. (a) Relative change in absorption coefficient $\Delta\alpha(\omega)$ of ZnTe as a function of the THz pulse 2 electric field. (b) Modulation factor versus the THz pulse 2 electric field, with error bars indicating repeated measurement uncertainties. (c) The modulation factor as a function of the pump fluence. (d) Modulation factor versus the time delay t_s of THz pulse 2.

fixed for all delay-dependent tests, and the scanning range of THz pulse 1 remained unchanged. The detected THz pulse 1 waveform can be modulated by varying the relative delay t_s, which is visualized in the color map presented in Fig. 3(e). Figure 3(f) shows that the reconstructed THz signal displays a waveform-like dependence on t_s upon THz pulse 2 pumping the ZnTe crystal. The maximum peak field of the reconstructed THz emission is recorded at $t_s = 3$ ps, which coincides with the peak position of THz pulse 2. By contrast, pronounced suppression of the THz signal is observed at $t_s = 2.16$ ps and $t_s = 3.49$ ps, corresponding to the negative valleys of the pumped THz pulse 2.

The frequency-resolved relative change in absorption spectra induced by THz pulse 2 excitation can be further extracted by comparing the THz spectra with and without THz pulse 2 excitation. Since positively polarized THz pump pulse 2 enhances the emitted THz signal, whereas negatively polarized excitation suppresses it, we further investigate the THz-field-dependent absorption of ZnTe to gain insight into the origin of the polarity- and field-dependent modulation. Fourier transforms are applied to the THz emission waveforms measured with and without THz pulse 2 excitation. As shown in Fig. 4(a), the relative change in absorption coefficient of ZnTe, $\Delta\alpha(\omega)$, is extracted,

$$\Delta\alpha(\omega) = \alpha_{\text{pump}}(\omega) - \alpha_0(\omega), \tag{4}$$

where α_{pump} and α_0 represent the THz absorption coefficients of ZnTe with and without THz pulse 2 excitation, respectively. The absorption coefficient is related to the extinction coefficient κ through $\alpha(\omega) = 4\pi\kappa(\omega)/\lambda$, where κ is obtained from the imaginary part of the complex refractive index $\tilde{n} = n + i\kappa$. When ZnTe is excited by positively polarized THz pulse 2, $\Delta\alpha$ is negative, which indicates reduced THz absorption after THz pumping rather than THz gain. In contrast, excitation with negatively polarized THz pump yields positive $\Delta\alpha$ and attenuates the detected THz pulse 1. As shown in Fig. 4(a), increasing the THz pump electric field enhances the absorption modulation amplitude, and the field polarity determines its sign.

To understand the microscopic origin of this absorption modulation, we first consider the THz absorption mechanism associated with the photoexcited carriers in ZnTe. Although the photon energy of the sampling pulse (1.55 eV) is below the bandgap of ZnTe, it can generate free carriers through two-photon absorption, populating electronic states near the conduction-band minimum. These photoexcited carriers strongly interact with the incident THz field, and their response can be described by the Drude model [40–42],

$$\hat{\varepsilon}(\omega) = \left(n + \frac{i\alpha c}{2\omega}\right)^2 = \varepsilon_{\text{dc}} - \frac{\omega_p^2}{\omega^2 - i\omega/\tau_r}, \tag{5}$$

where n and α are the frequency-dependent refractive index and absorption coefficient, respectively; τ_r is the carrier momentum relaxation time; and ε_{dc} is the background dielectric constant of the semiconductor in the absence of free carriers [21]. $\omega_p = (Ne^2/\varepsilon_0 m)^{1/2}$ is the plasma frequency, where e is the elementary charge, N is the free-carrier density, ε_0 is the vacuum permittivity, and m is the carrier effective mass. According to Eq. (5), the plasma frequency governs the strength of free-carrier THz absorption. Nonlinear THz response in doped or photoexcited semiconductors could originate from THz-field-induced carrier heating, which modifies the plasma frequency and consequently the THz absorption [43]. In the limiting case of $\omega_p \to 0$, the free-carrier contribution to THz absorption vanishes. A reduction in ω_p can be achieved through an increase in the carrier effective mass m. This can occur through redistribution of conduction-band electrons: electrons transfer from low-momentum, light-effective-mass states near the Γ-valley minimum to high-momentum, heavy-effective-mass states in satellite valleys [21]. ZnTe hosts multiple conduction-band valleys. Electrons residing near the Γ-valley minimum carry an effective mass of $m_\Gamma \approx 0.12m_0$, while the L and X valleys feature larger values: $m_L = 0.46m_0$ and $m_X = 0.30m_0$ [44].

Therefore, intervalley transfer would increase the average carrier effective mass. At electric fields near the static Gunn field (~100 kV/cm), carriers can populate high-energy conduction-band states. However, the peak THz field employed in the present work (~0.8 kV/cm) is approximately two orders of magnitude lower than the Gunn field, suggesting that intervalley scattering is not expected to be the dominant mechanism under the present excitation conditions.

Besides intervalley scattering, another possible mechanism is phonon bleaching associated with ladder climbing [45]. Since phonon bleaching originates from the redistribution of vibrational-state populations under intense THz excitation, it is primarily determined by the amplitude rather than the polarity of the driving field. Therefore, this mechanism cannot explain the observed polarity-dependent response. Moreover, the peak THz field employed here is several orders of magnitude lower than the field strengths reported to induce ladder climbing [45], making this mechanism less likely under our experimental conditions. These results instead indicate an intrinsic process governed by the polarity of the driving THz field.

Prior THz-pump and optical-probe measurements suggest negligible second-order nonlinearity of ZnTe at optical frequencies [46,47]. However, phonon resonances enable pronounced second-order nonlinear responses of crystals under THz excitation [48,49]. Therefore, for the TPTP measurement in ZnTe, the second-order nonlinear response in the THz regime is non-negligible. Thus, $E_{\mathrm{THz}}(t_{\mathrm{p}})$ can be described [31],

$$E_{\mathrm{THz}}(t_{\mathrm{p}}) = E_{\mathrm{THz},1}(t_{\mathrm{p}}) + \theta(t_{\mathrm{p}} - t_0) \cdot [A \times E_{\mathrm{THz},1}(t_{\mathrm{p}}) E_{\mathrm{THz},2}(t_{\mathrm{p}}) + B \times E_{\mathrm{THz},1}(t_{\mathrm{p}}) E^2_{\mathrm{THz},2}(t_{\mathrm{p}})], \tag{6}$$

where $E_{\mathrm{THz},1}(t_{\mathrm{p}})$ is the emitted THz pulse 1 without the THz pumping pulse 2, and $E_{\mathrm{THz},2}(t_{\mathrm{p}})$ is the THz pulse 2. $\theta(t_{\mathrm{p}} - t_0)$ is a half-window Heaviside function, where t_0 denotes the first arrival time of the THz pulse 2. The coefficient A is related to the second-order nonlinear susceptibility $\chi^{(2)}$, and B is related to the third-order nonlinear susceptibility $\chi^{(3)}$. The modulation factor can be defined as the ratio between the peak field with the THz pulse 2 incident on the ZnTe crystal and the peak field of the original THz pulse 1 without the THz pulse 2: Modulation factor $= E_{\mathrm{THz}}(t_{\mathrm{p}})/E_{\mathrm{THz},1}(t_{\mathrm{p}})$. As illustrated in Fig. 4(b), the modulation factor varies from 0.32 ± 0.01 to 5.39 ± 0.28 as the peak electric field of the THz pump pulse 2 is increased from −260 to 800 V/cm. The increasing trend deviates from linearity. The measured modulation factor can be described as

$$\text{Modulation factor} \propto 1 + A \times E_{\mathrm{THz},2} + B \times E^2_{\mathrm{THz},2}. \tag{7}$$

This model reproduces the key features of the experimental data and confirms the quadratic relationship predicted by Eq. (7). As shown in Fig. 4(b), the experimental results are well described by the superposition of a linear term proportional to $E_{\mathrm{THz},2}$ (blue curve) and a quadratic term proportional to $E^2_{\mathrm{THz},2}$ (red curve). The fitted coefficients are $A = (2.84 \pm 0.27) \times 10^{-7}$ m/V and $B = (3.25 \pm 0.41) \times 10^{-14}$ m^2/V^2, revealing the respective contributions of the Pockels and Kerr effects to the observed nonlinear response in ZnTe, consistent with the field-dependent behavior reported in our previous work [50]. It should be noted that the fitted coefficients are influenced by the crystal thickness and detection geometry. In addition, the THz field strength employed in our experiment is two orders of magnitude lower than that used in previous studies [31], which prevents an accurate determination of the intrinsic nonlinear susceptibilities. The observed first- and second-order THz-field-dependent modulation, together with the polarity-sensitive response, directly evidences the coexistence of Pockels and Kerr effects in ZnTe. Since the Kerr contribution is an even-order term, it remains unchanged upon reversal of the polarity of the THz pump pulse 2. In contrast, the linear Pockels contribution changes sign from $+E_{\mathrm{THz},2}$ to $-E_{\mathrm{THz},2}$, thereby increasing or decreasing the total nonlinear modulation of the detected THz pulse 1. As a result, this polarity-dependent sign reversal of the linear Pockels contribution accounts for the experimentally observed polarity dependence of the THz-field-induced absorption modulation. In future work, stronger THz fields generated by optimized approaches, such as the tilted-pulse-front technique, will be explored to enable a more accurate quantitative determination of the intrinsic second- and third-order nonlinear susceptibilities $\chi^{(2)}$ and $\chi^{(3)}$ of ZnTe.

With the modulation mechanism clarified, we finally characterize its tunability across experimental parameters. As plotted in Fig. 4(c), the modulation factor decreases from 4.18 ± 0.68 to 2.43 ± 0.19 with the growing amplitude of THz pulse 1 (optical pump fluence 0.56–2.83 mJ/cm^2). Figure 4(d) illustrates the modulation factor's dependence on the delay t_{s}, which is tuned by scanning the sampling optical pulse to access different instantaneous THz pump pulse 2 fields in the ZnTe crystal. In this manner, the effective sampling time is shifted, enabling the ZnTe crystal to experience THz pump pulse 2 electric fields with different amplitudes and polarities at each t_{s}, thereby modulating THz pulse 1 through Eq. (7). At $t_{\mathrm{s}} = 3$ ps, where THz pulse 2 reaches positive polarity and maximum amplitude, the modulation factor reaches its maximum value. Finally, we note that our finding highlights the importance of considering the nonlinear response of electro–optic detectors in ultrafast THz spectroscopy experiments. The ZnTe crystal acts as an active nonlinear element; therefore, any THz pulse co-propagating with the THz probe pulse can modify the effective detection sensitivity through additional nonlinear electro–optic interactions. To minimize such detection-induced artifacts, TPTP experiments should employ a thinner ZnTe crystal, a different detection crystal with lower $\chi^{(2)}$, or non-collinear propagation configurations for the THz pump and THz probe beams. In addition, reference measurements are also required to separate intrinsic material responses from detector-induced nonlinear contributions.

In summary, we reveal that the apparent enhancement of the measured THz signal in TPTP measurements originates from the linear and nonlinear electro–optical response of the ZnTe detection crystal rather than the Fe_4GeTe_2 THz emitter. The observed modulation can be consistently understood through the interplay between effective second- and third-order nonlinearities, in which the polarity-sensitive Pockels response accounts for the enhancement and suppression of the detected THz signal, while the Kerr response provides additional nonlinear corrections. More broadly, our work redefines the role of electro–optic detection crystals in THz experiments. Rather than serving as purely passive detection, they should be regarded as active nonlinear optical media that participate in the detected THz-field. These findings highlight the potential of intrinsic material nonlinearities for nonlinear manipulation of THz radiation, opening new avenues for the development of nonlinear THz photonics and ultrafast optoelectronic technologies.

Additional Information

Correspondence and requests for materials should be addressed to Zuanming Jin, Tianxiao Nie, Yan Peng, or Yiming Zhu.

Acknowledgements

This work was supported by the National Key Research and Development Program of China (Grant Nos. 2023YFF0719200 and 2023YFF0717900), the National Natural Science Foundation of China (Grant Nos. 62588201, 62322115, U24A20226, 62422510, 62435010, 62335012, 61988102, W2411060, and 62274009), the 111 Project (Grant No. D18014), the Shanghai Educational Development Foundation (Grant No. 24SG46), the Major Basic Research Program of Shandong Provincial Natural Science Foundation (Grant No. ZR2026ZD26), the Science and Technology Commission of Shanghai Municipality (Grant No. 22JC1400200), the Beijing Municipal Natural Science Foundation (Grant No. Z230004), the General Administration of Customs People's Republic of China (Grant No. 2019HK006), and the State Assignment of Lomonosov Moscow State University and the State Assignment of NRC "Kurchatov Institute".

References

[1] Franken P A, Hill A E, Peters C W, and Weinreich G 1961 *Phys. Rev. Lett.* **7** 118
[2] Yeh K L, Hoffmann M C, Hebling J, and Nelson K A 2007 *Appl. Phys. Lett.* **90** 171121
[3] Hebling J, Yeh K L, Hoffmann M C, and Nelson K A 2008 *IEEEJ. Sel. Top. Quantum Electron.* **14** 345
[4] Hoffmann M C and Fulop J A 2011 *J. Phys. D: Appl. Phys.* **44** 083001
[5] Chong M Z, Zhou Y W, Zhang Z K, Zhao J, Zhang Y Y, Zhang C Q, Zang X F, Du C H, Liu P K, and Xia M Y 2024 *Light: Advanced Manufacturing* **5** 38
[6] Peng Y, Shi C J, Zhu Y M, Gu M, and Zhuang S L 2020 *PhotoniX* **1** 12
[7] Fan J, Liu Q H, Huang Z, and Zhang Y 2025 *Electromagnetic Science* **3** 0110332
[8] Cai M, Zhang J H, Chen Y B, Hong L, Fu J J, Zheng X G, Yao Y F, Zhang S C, Liu Y J, Dong B Y, Chen S, Li P, You G J, Zhang J W, Guo X G, Zhu Y M, and Zhuang S L 2025 *Sci. Adv.* **11** eadv0768
[9] Ganichev S and Prettl W 2005 *Intense Terahertz Excitation of Semiconductors* (Oxford: Oxford University Press)
[10] Danielson J R, Lee Y S, Prineas J P, Steiner J T, Kira M, and Koch S W 2007 *Phys. Rev. Lett.* **99** 237401
[11] Hirori H, Nagai M, and Tanaka K 2010 *Phys. Rev. B* **81** 081305
[12] Wen H, Wiczer M, and Lindenberg A M 2008 *Phys. Rev. B* **78** 125203
[13] Hoffmann M C, Hebling J, Hwang H, Yeh K L, and Nelson K 2009 *Phys. Rev. B* **79** 161201
[14] Su F H, Blanchard F, Sharma G, Razzari L, Ayesheshim A, Cocker T L, Titova L V, Ozaki T, Kieffer J C, Morandotti R, Reid M, and Hegmann F A 2009 *Opt. Express* **17** 9620
[15] Hebling J, Hoffmann M C, Hwang H Y, Yeh K L, and Nelson K A 2010 *Phys. Rev. B* **81** 035201
[16] Sharma G, Razzari L, Su F H, Blanchard F, Ayesheshim A, Cocker T L, Titova L V, Bandulet H C, Ozaki T, Kieffer J C, Morandotti R, Reid M, and Hegmann F A 2010 *IEEE Photonics J.* **2** 578
[17] Hoffmann M C, Monozon B S, Livshits D A, Rafailov E U, and Turchinovich D 2010 *Appl. Phys. Lett.* **97** 231108
[18] Hoffmann M C, Hebling J, Hwang H Y, Yeh K L, and Nelson K A 2009 *J. Opt. Soc. Am. B* **26** A29
[19] Blanchard F, Golde D, Su F H, Razzari L, Sharma G, Morandotti R, Ozaki T, Reid M, Kira M, Koch S W, and Hegmann F A 2011 *Phys. Rev. Lett.* **107** 107401
[20] Liu M, Hwang H Y, Tao H, Strikwerda A C, Fan K, Keiser G R, Sternbach A J, West K G, Kittiwatanakul S, Lu J, Wolf S A, Omenetto F G, Zhang X, Nelson K A, and Averitt R D 2012 *Nature* **487** 345
[21] Turchinovich D, Hvam J M, and Hoffmann M C 2012 *Phys. Rev. B* **85** 201304
[22] Ho I C and Zhang X C 2013 *IEEE J. Sel. Top. Quantum Electron.* **19** 8401005
[23] Yumoto G, Matsunaga R, Hibino H, and Shimano R 2018 *Phys. Rev. Lett.* **120** 107401
[24] Cai J, Chen S, Geng C, Li J, Quan B, and Wu X J 2023 *Nanophotonics* **12** 2517
[25] Sai P, Korotyeyev V V, But D B, Dub M, Yavorskiy D, Łusakowski J, Słowikowski M, Kukhtaruk S, Liashchuk Y, Han J W, Böttger C, Pashkin A, Winnerl S, Knap W, and Mittendorff M 2025 *Adv. Opt. Mater.* **13** 2500716
[26] Yoshioka D, Sekiguchi F, Yoshikawa N, and Shimano R 2025 *Nano Lett.* **25** 13764
[27] Hafez H A, Chai X, Ibrahim A, Mondal S, Férachou D, Ropagnol X, and Ozaki T 2016 *J. Opt.* **18** 093004
[28] Jin Z W, Lou J, Shu F Z, Hong Z, and Qiu C W 2025 *Research* **8** 0562
[29] Liu S J, Lu C H, Fan Z Q, Wang S X, Li P Y, Chen X H, Pan J, Xu Y, Liu Y, and Wu X J 2022 *Appl. Phys. Lett.* **120** 172404
[30] Qu X M, Huang Y D, Zhou B, Gao M X, Lou J, Feng Y F, Zhao Z X, Chang C, Shkurinov A P, and Verboncoeur J 2024 *Optica* **11** 1478
[31] Selz F, Kölbel J, Paries F, von Freymann G, Molter D, and Mittleman D M 2025 *Opt. Express* **33** 9575
[32] Jin Z M, Hong H X, Sun Y, Li Z S, Li J, Peng J Y, Nie T X, Peng Y, Zhang C, Balakin A V, Shkurinov A P, Zhu Y M, and Zhuang S L 2025 *Adv. Opt. Mater.* **13** e00951
[33] Lan Z Q, Jin Z M, Wang S H, Wang Y F, Li H Y, Ye C, Lu B, Guo Y Y, Li Z S, Balakin A V, Shkurinov A P, Peng Y, Zhu Y M, and Zhuang S L 2026 *Newton* **2** 100516
[34] Guo Y Y, Chen Z Q, Jin Z M, Wang X F, Zhang C, Balakin A V, Shkurinov A P, Peng Y, Zhu Y M, and Zhuang S L 2024 *Adv. Funct. Mater.* **34** 2407749
[35] Jin Z M, Peng Y, Fang Y Q, Ye Z J, Fan Z Y, Liu Z L, Bao X C, Gao H, Ren W, Wu J, Ma G H, Chen Q L, Zhang C, Balakin A V, Shkurinov A P, Zhu Y M, and Zhuang S L 2022 *Light Sci. Appl.* **11** 209
[36] Planken P C M, Nienhuys H K, Bakker H J, and Wenckebach T 2001 *J. Opt. Soc. Am. B* **18** 313
[37] Zhao G, Schouten R N, van der Valk N, Wenckebach W Th, and Planken P C M 2002 *Rev. Sci. Instrum.* **73** 1715
[38] Chen Z Q, Qiu H S, Cheng X J, Cui J Z, Jin Z M, Tian D, Zhang X, Xu K K, Liu R X, Niu W, Zhou L Q, Qiu T Y, Chen Y Q, Zhang C H, Xi X X, Song F Q, Yu R, Zhai X C, Jin B B, Zhang R, and Wang X F 2024 *Nat. Commun.* **15** 2605
[39] Wang Y F, Jin Z M, Cai M, Lan Z Q, Ge Z J, Feng Z, Tan W, Balakin A V, Shkurinov A P, Peng Y, and Zhu Y M 2026 *Adv. Sci.* **13** e75727
[40] Huber R, Tauser F, Brodschelm A, Bichler M, Abstreiter G, and Leitenstorfer A 2001 *Nature* **414** 286
[41] Dressel M and Grüner G 2002 *Electrodynamics of Solids: Optical Properties of Electrons in Matter* (Cambridge: Cambridge University Press)
[42] Deng H, Chen L Y, Qu W W, Liu Q C, Danso S, and Shang L P 2020 *Opt. Eng.* **59** 056101
[43] Peng R J, Jin Z M, Jiang Y X, Zhang H P, He W, and Peng Y 2026 *Nanomaterials* **16** 530
[44] Khedim S, Chabane Sari N E, Benyoucef B, and Bouazza B 2011 *Mater. Sci. Appl.* **2** 364
[45] Jewariya M, Nagai M, and Tanaka K 2010 *Phys. Rev. Lett.* **105** 203003
[46] Tian Z, Wang C L, Xing Q R, Gu J Q, Li Y F, He M X, Chai L, and Wang Q Y 2008 *Appl. Phys. Lett.* **92** 041106
[47] Caumes J P, Videau L, Rouyer C, and Freysz E 2002 *Phys. Rev. Lett.* **89** 047401
[48] Dolgaleva K, Materikina D V, Boyd R W, and Kozlov S A 2015 *Phys. Rev. A* **92** 023809
[49] Zibod S, Rasekh P, Yildrim M, Cui W, Bhardwaj R, Ménard J M, Boyd R W, and Dolgaleva K 2023 *Adv. Opt. Mater.* **11** 2202343
[50] Li D N, Guo Y Y, Jin Z M, Dong X M, Zhang C, Balakin A V, Shkurinov A P, Peng Y, Zhu Y M, and Zhuang S L 2024 *Appl. Phys. Lett.* **125** 051103